Fe-Ti oxide micro-inclusions in clinopyroxene of oceanic gabbro: phase content, orientation relations and petrogenetic implication

Olga Ageeva[1,2], Gerlinde Habler[1], Alexey Pertsev[2], & Rainer Abart[1]

[1] University of Vienna, Department of Lithosphere Research, Althanstrasse 14, 1090 Wien, Austria

[2] Institute of Geology of Ore Deposits, Petrography, Mineralogy, and Geochemistry (IGEM), Staromonetnyi 35, Moscow, 119017, Russia

Corresponding author: olga.ageeva@univie.ac.at

INTRODUCTION

Oriented micro-inclusions of Fe-Ti oxides such as magnetite, ulvospinel, hematite, and ilmenite that are hosted in rock-forming silicate minerals like plagioclase and pyroxene are a widespread phenomenon in igneous rocks (Poldervaart and Gilkey, 1954; Divljan, 1960; Neumann and Christie, 1962; Amburstmacher and Banks, 1974; Sobolev, 1990; Usui et al.,

1

27 2006; Wenk et al., 2011; Ageeva et al., 2016 and others). Due to their small size these

28 inclusions often have single magnetic domain state and unusually stable magnetization. Their

29 stable magnetization and protection from external influence by the mineral-host crystal make

30 these micro-inclusions important carriers of the paleomagnetic record (Hargraves and Young,

31 1969; Xu and others, 1997; Renne et al., 2002; Harrison et al., 2002; Smirnov et al., 2003;

32 Feinberg et al., 2005 and others).

33   The presence of Fe-Ti oxide micro-inclusions in rock-forming minerals is usually

34 attributed to exsolution from the host phase. Special conditions predetermine their

35 appearance. Initial crystallization, re-crystallization or alteration of the potential silicate host

36 mineral in a high-temperature magmatic or metamorphic environment allows iron and

37 titanium to be incorporated into the silicate lattice at high concentrations. Subsequent cooling,

38 possibly fluid mediated re-crystallization at lower temperature, or at different oxygen fugacity

39 may render the silicate phase supersaturated with respect to Fe-Ti oxide phases and may

40 induce precipitation of Fe-Ti oxides within the silicate host crystal (Smith, 1974).

41   Once precipitated the micro-inclusions may undergo various changes like internal

42 exsolution, re-crystallization, or chemical changes. It is known that Fe-Ti oxides are highly

43 sensitive to redox state (Sauerzapf et al., 2008; Dégi et al., 2009). When enclosed in a more

44 stable silicate host, the Fe-Ti oxides are less strongly exposed to changes in their geochemical

45 environment and somewhat more sheltered from hydration and low-temperature hydrothermal

46 alteration than the matrix phases. Therefore, the phase contents, chemical compositions and

47 microstructures of the inclusions likely reflect the evolution of pressure, temperature and

48 redox state during their primary crystallization and early evolution. Their shape orientation

49 relationships (SORs) and their crystallographic orientation relationships (CORs) with their

50 mineral hosts provide important constraints on the formation mechanisms and on

51 transformations that the micro-inclusions may have undergone. Combined with the

52 mineralogical and chemical compositions of both the micro-inclusions and the mineral host,

53 the SORs and CORs provide the basis for using Fe-Ti oxide micro-inclusions as indicators of

54 post-crystallization conditions and for extracting petrogenetic, petromagnetic and

55 paleomagnetic information.

56

57   *Clinopyroxene hosted Fe-Ti oxide micro-inclusions*

58   In this study we address Fe-Ti oxide micro-inclusions hosted in gabbroic

59 clinopyroxene. In particular, we focus on the crystallographic- and shape orientation

60 relationships between the Fe-Ti oxide micro-inclusions and the host clinopyroxene and try to

61 link different types of the inclusions to specific stages of the petrogenetic evolution. It has

62 been shown earlier (Bown and Gay, 1959; Okamura et al., 1976; Harlow and Klimentidis,

63 1980; Fleet et al., 1980; Woensdregt et al., 1983; Doukhan et al., 1990; Renne et al., 2002;

64 Feinberg, et al., 2004; Hwang et al., 2010) that: (i) there are only two types of shape

65 orientation and corresponding CORs of needle-shaped magnetite inclusions in a

66 clinopyroxene host. Both types are represented by Fe-Ti micro-inclusions that are flattened

67 parallel to the (010) planes of the clinopyroxene host; (ii) according to their elongation

68 subparallel either to clinopyroxene [100] or to clinopyroxene [001] these two types are

69 referred to as X- and Z-type inclusions, respectively (Fleet et al., 1980); (iii) based on the

70 notion that the angle between the needle long-axes of the X- and Z-type inclusions depends on

71 their formation temperature, a geo-thermometer has been calibrated that reveals the

72 temperature of exsolution of the Fe-Ti oxide micro-inclusions from clinopyroxene (Fleet et

73 al., 1980; Doukhan et al., 1990; Feinberg et al., 2004). This temperature is of pivotal

74 importance in the context of petrogenetic and paleomagnetic reconstructions.

75

76   *Fe-Ti oxides in the lower oceanic crust*

77   The Fe-Ti oxide micro-inclusions in rock-forming minerals of modern oceanic crust

78 gabbros are particularly interesting, since these associations often show a multistage

79   magmatic history and interaction with evolved residual melts enriched in Fe and Ti (e.g.,

80   Natland et al., 1991; Malpas and Robinson, 1997; Grimes et al., 2008; Hayman et al., 2011;

81   Hekinian, 2014). This leads to the crystallization of Fe-Ti oxide macro-grains and possibly to

82   the enrichment of the rock-forming silicates in Fe and Ti. The crystallization of Fe-Ti oxide

83   macro-grains in oceanic gabbro and the provenance of residual liquids enriched in Fe and Ti,

84   as a result of MORB-type magma differentiation, redox state, and synmagmatic deformation

85   have been debated for many years (e.g., Natland et al., 1991; Agar and Lloyd, 1997; Dick et

86   al, 2000). However, the detailed evolution of the Fe-Ti oxide micro-inclusions in the rock-

87   forming silicates from oceanic gabbros does not seem to have received sufficient attention.

88   In this communication we focus on the evolution of clinopyroxene-hosted Fe-Ti

89   oxide micro-inclusions in oceanic gabbro that was dredged from the Mid Atlantic ridge at

90   10°42.95′N, 41°34.60′W. An earlier study (Pertsev et al., 2015) suggests that the

91   petrogenetic history of the gabbro includes late magmatic crystallization of Fe-Ti oxides,

92   interaction between a crystal aggregate and residual liquid, and multistage hydrothermal

93   alteration. We report on the shape and crystallographic orientation relationships between Fe-

94   Ti oxide micro-inclusions, associated amphibole lamellae and a clinopyroxene host. Different

95   types of Fe-Ti oxide micro-inclusions are shown and their attribution to different formation

96   mechanisms is discussed. The temperature of primary formation of the inclusions is inferred

97   based on the geo-thermometer by Fleet et al. (1980) and Feinberg et al. (2004). Multistage

98   phase transformations of the Fe-Ti oxide inclusions are ascribed to changes in temperature

99   and redox regimes during the evolution of the gabbro. The genetic relations between the Fe-Ti

100   oxide micro-inclusions and the associated amphibole lamellae are discussed in terms of

101   possible processes of exsolution and intra-crystalline re-distribution of components in the

102   clinopyroxene host during the late-magmatic and hydrothermal stages. Although the results

103   have been obtained from a single sample, the proposed approach is generally applicable and

104   helps to unravel the provenance and evolution of different gabbro assemblages from modern

105   oceanic crust and ophiolites.

106

107   SAMPLE

108   The gabbro sample – L2612-41 (gabbro-41) – was collected together with more

109   abundant mantle-derived peridotites from the Vema lithospheric section, Central Atlantic

110   (Auzende et al., 1989; Bonatti et al., 2003, 2005) by dredging at 10°42.95′N, 41°34.60′W,

111   5195-4620 mbsl (Cipriani et al., 2009). This gabbro-peridotite assemblage was formed close

112   to or within the crust–mantle transition zone near the end of a slow-spreading segment, where

113   thin igneous crust and underlying mantle were affected by intense fracturing and

114   hydrothermal alteration during interaction with seawater (Pertsev et al., 2015).

115   A detailed mineralogical and petrographic description, including fluid inclusion data

116   of gabbro-41 is available in Pertsev et al. (2015). The main petrogenetic stages reconstructed

117   by the latter authors include: (i) early magmatic crystallization of plagioclase + augite ±

118   enstatite; (ii) late magmatic formation of Ti-bearing hornblende, Fe-Ti oxides and local re-

119   crystallization of plagioclase and augite related to reaction with residual melt at 800-900°C;

120   (iii) early hydrothermal alteration due to interaction with a reducing fluid that was generated

121   by seawater/peridotite interaction; hydrothermal alteration occurred at 560-640°C and caused

122   local crystallization of chlorine-bearing ferropargasite-ferroedenite, formation of olivine

123   coronas between enstatite and magnetite, local enrichment of the anorthite component in

124   plagioclase and replacement of augite by diopside; and (iv) late hydrothermal alteration

125   related to tectonic unroofing and infiltration of seawater or slightly modified seawater (3-9%

126   NaCl) which lead to the formation of albite, chlorite, and actinolite.

127

128   METHODS

129   The main methods used in this study apart from optical polarization microscopy are

130   Scanning Electron Microscopy (SEM) including Electron BackScatter Diffraction analysis

131   (EBSD), Electron Probe MicroAnalysis (EPMA), and Universal stage measurements. All

132   methods are described in detail in the Appendix 1.

133

134   RESULTS

135   *Gabbro mineralogy*

136   The gabbro-41 sample is mainly composed of coarse-grained (3-7 mm sized) primary

137   magmatic plagioclase Pl_1 (An# 44-45), clinopyroxene Cpx_1 (augite), and minor

138   orthopyroxene, which all together represent more than 90% of the rock volume. Bent parting

139   cracks in Cpx_1, banded optical extinction of Pl_1, and local crystal-plastic deformation features

140   in plagioclase and clinopyroxene indicate deformation, which probably occurred during the

141   late-magmatic stage. The late-magmatic mineral assemblage is represented by large interstitial

142   grains of Fe-Ti oxides, a $Hbl + Cpx_2 + Pl_2$ assemblage and by $Cpx_2 + Hbl \pm Mt$ micro-

143   aggregates partially replacing early magmatic clinopyroxene Cpx_1 (Pertsev et al., 2015). The

144   late magmatic hornblende (titanian pargasite) is brown and often occurs as blebs in a

145   clinopyroxene host. The late-magmatic plagioclase has higher anorthite (An# 55-63) and

146   LREE contents than the early magmatic plagioclase Pl_1 (An#43) (Pertsev et al., 2015). Early

147   hydrothermal hornblende fills a network of cracks within plagioclase Pl_1 and is accompanied

148   by re-deposited plagioclase Pl_3. It clearly differs in color from late magmatic titanian

149   hornblende and shows pleochroism from dark green to greenish yellow. It is enriched in Fe^{2+}

150   (Mg# 0.5 to 0.25) and Cl (0.4-1.4 wt.%). This hornblende is mantled by re-deposited

151   plagioclase, which is enriched in anorthite (An# 49-52) and Sr relative to Pl_1 (Pertsev et al.,

152   2015). Late albite, chlorite, and actinolite are observed along grain boundaries and in parting

153   cracks of pre-existing clinopyroxene and are ascribed to a late hydrothermal overprint.

154   In gabbro-41 Fe-Ti oxide micro-inclusions are observed in minerals of different

155   genetic groups including (i) early magmatic plagioclase and clinopyroxene, (ii) late-magmatic

156   plagioclase and clinopyroxene, and (iii) late-hydrothermal actinolite lamellae in

157   clinopyroxene. In this paper we present the results from the clinopyroxene-hosted inclusions.

158   The abbreviations of mineral names correspond to those used by Pertsev et al. (2015).

159

160   *The Fe-Ti oxide micro-inclusions in clinopyroxene: types, distribution and SORs*

161   Rock-forming clinopyroxene of gabbro-41 contains micro-inclusions of Fe-Ti

162   oxides, which mostly take the form of needles or elongated plates or blades flattened parallel

163   to and lying in the (010) plane of the clinopyroxene host (Fig. 1, Fig. 2). The inclusions

164   consist of composite Fe-Ti oxide assemblages containing magnetite + ulvospinel, magnetite +

165   ilmenite + ulvospinel, or magnetite + ilmenite assemblages. Pure magnetite inclusions are

166   rare. Typically, the inclusions are only 0.2 – 2 micrometers thick in the [010] direction of their

167   mineral host, a few micrometers wide and 10-100 micrometers long. In sections parallel to the

168   (010) plane of the clinopyroxene host the Fe-Ti oxide micro-inclusions show two distinct

169   elongation directions. The more abundant elongation direction is sub-parallel to the [001]-

170   direction of the clinopyroxene host, the less abundant elongation direction is sub-parallel to

171   the [100]-direction of the clinopyroxene host. Following Bown and Gay (1959) we refer to the

172   two elongation directions as X-type and Z-type inclusions, respectively.

173   The distribution of the Fe-Ti oxide micro-inclusions is not uniform. The more

174   abundant Z-type inclusions tend to be closely associated with 0.01 to 5 micrometers wide

175   hornblende (Hbl) lamellae extending parallel to the (010) plane of the clinopyroxene host

176   (Fig. 1b, Fig. 2a, c). The amphibole lamellae reach their maximum width near the Fe-Ti oxide

177   micro-inclusions and taper out at some distance from the inclusions. On a larger scale, the Z-

178   type inclusions tend to be concentrated along (100) planes of clinopyroxene (Fig. 1b, Fig. 3b).

179   The less abundant X-type inclusions are primarily observed near big cracks or near the

180 contacts of the clinopyroxene host to large interstitial grains of Fe-Ti oxides, where they occur

181 together with Z-type inclusions (Fig. 1a). Like the Z-type inclusions, the X-type inclusions are

182 usually also accompanied by hornblende lamellae.

183 A separate generation of homogeneous ilmenite inclusions is associated with the actinolite

184 lamellae lying in the (100) plane of the clinopyroxene host. The ilmenite inclusions take the

185 form of large plates lying in the (100) plane of the actinolite, which are 50 - 100 microns

186 wide. The shape orientation relationships of hornblende (Hbl) and actinolite (Ac) lamellae in

187 the clinopyroxene host as well as the shape orientation relationships of the Fe-Ti micro-

188 inclusions are shown schematically in Figure 1 b.

189

190 *Crystallographic and shape orientation relations*

191 The (010)-oriented hornblende and (100)-oriented actinolite lamellae have identical

192 crystallographic orientations and show strong CORs with the clinopyroxene host. The (010)

193 and (100) planes of clinopyroxene and amphibole are parallel to each other (Table 1), and the

194 (001) plane of the clinopyroxene is parallel to the (10-1) plane of the amphiboles.

195 The crystallographic orientation relationships between the Fe-Ti oxide phases in the

196 inclusions and the clinopyroxene host are also strong (Table 1, Fig. 4, Fig. 5, Fig. 6). In both

197 the X- and Z- type inclusions the (110) plane of magnetite is parallel to the (010) plane of the

198 clinopyroxene host. In addition, one of the (111) planes of magnetite is parallel to the (-101)

199 plane of the clinopyroxene host in the X-type inclusions, and one of the (111) planes of

200 magnetite is parallel to the (100) plane of the clinopyroxene host in the Z-type inclusions.

201 These crystallographic orientation relationships together with the X- and Z-type shape

202 orientations were first described by Bown and Gay (1959), and have been documented

203 repeatedly since then (Bown and Gay, 1959; Okamura et al., 1976; Harlow and Klimentidis,

204 1980; Fleet et al., 1980; Woensdregt et al., 1983; Doukhan et al., 1990; Renne et al., 2002;

205 Feinberg, et al., 2004; Hwang et al., 2010). The symmetrically equivalent CORs between X-

206 and Z-type magnetite inclusions and the clinopyroxene host are summarized in Table 1 and

207 are illustrated in Figure 4.

208   Despite the fact that the CORs between the Fe-Ti oxide micro-inclusions and the

209 clinopyroxene host are strong, they do not correspond to the shape elongation directions of the

210 Fe-Ti oxide micro-inclusions. Optical measurements with the universal stage microscope

211 showed that the angles between the long axes of the two sets of needle-shaped magnetite X-

212 and Z-type inclusions vary in the narrow range of 106-107°.

213   The homogeneous ilmenite grains take the form of plates extending parallel to the

214 (001) plane of the ilmenite and oriented parallel to the actinolite lamella boundaries (Fig. 2 b).

215 The ilmenite inclusions show strong CORs with their actinolite host, where the CORs

216 correspond to those of the Z-type inclusions (Fig. 6, Table 1).

217

218   *Shape and crystallographic orientation relationships inside of heterogeneous micro-*

219 *inclusions*

220   In the composite Fe-Ti oxide micro-inclusions the intergrown phases show strong

221 crystallographic orientation relationships. Magnetite and ulvospinel have identical

222 crystallographic orientations. Ilmenite adheres to the common ilmenite – magnetite mutual

223 COR with one of the (111) planes of magnetite parallel to the (001) plane of ilmenite and

224 three of the (110) planes of magnetite parallel to the three (100) planes of ilmenite.

225   The inclusions that consist of magnetite-ulvospinel intergrowths show internal

226 graphic microstructure (Fig. 2 b). The magnetite-ulvospinel phase boundaries are mainly

227 parallel to the {100} planes of the magnetite, which is the most common interface orientation

228 in magnetite-ulvospinel intergrowths (Ramdohr, 1955).

229   Whereas the ulvospinel phase of the Usp-Mt intergrowths is homogeneous, the

230 magnetite shows a lamellar internal microstructure, which is due to the presence of sub-

231 micron wide lamellae of supposedly ulvospinel oriented parallel to one of the {100} planes of

232 the magnetite host (Fig. 2 b). The phase boundaries between the inclusions and the pyroxene

233 host as well as the phase boundaries between the intergrown magnetite and ulvospinel phases

234 inside the inclusions are generally straight. In contrast, when magnetite is accompanied by

235 ilmenite instead of or in addition to ulvospinel, the phase boundaries within the inclusions are

236 uneven and give the impression that the phases are corroded (Fig. 2 c, Fig. 3 a). The corrosion

237 of the magnetite-ilmenite inclusions is particularly pronounced in the vicinity of cracks

238 following the clinopyroxene parting planes.

239

240 *Mineral host composition*

241 The Fe-Ti oxide inclusions are mainly located in large grains of clinopyroxene,

242 which were identified as the early-magmatic 'Cpx$_1$' generation by Pertsev et al., (2015)

243 (Table 2, an. 1, 2). The Fe-Ti micro-inclusions in Cpx$_1$ are spatially related to amphibole

244 lamellae. The (010) amphibole lamellae (Table 2, an. 5) that are linked to the multiphase X-

245 and Z-type inclusions are closely similar to the Al- and Ti-rich hornblende (titanian pargasite)

246 "Hbl$_2$" (Table 2, an. 6) described in (Pertsev et al., 2015).

247 In the domains where the hornblende lamellae are associated with the "X"- and "Z"-

248 type inclusions, the composition of the clinopyroxene host is slightly changed compared to

249 the bulk Cpx$_1$ and in terms of composition corresponds to the late-magmatic clinopyroxene

250 'Cpx$_2$' (Table 2, an. 3, 4). Both Cpx$_1$ and Cpx$_2$ are classified as augite. However, Cpx$_2$, which

251 is associated with the hornblende lamellae, is slightly depleted in Al, Ti and Na and enriched

252 in Si, Ca and Mg with respect to Cpx$_1$ (Table 2, an.1 and 3; Fig. 7). Nevertheless the

253 concentration of Fe is the same in Cpx$_1$ and Cpx$_2$.

254 The amphibole lamellae (Table 2, an. 9) that have a shape preferred orientation

255 parallel to the Cpx (100) plane and which host the platy ilmenite inclusions are classified as

256 actinolite (Al^{IV} 0.1 to 0.2, atoms per formula unit). Yet, actinolite lamellae contain irregularly

257 distributed domains of variable hornblende composition with higher concentrations of Al, Fe,

258 and Cl (up to 7.9, 26.0, and 0.02 wt.% respectively (Table 2, an. 7). The ilmenite micro-

259 inclusions in actinolite (Table 2, an. 12) are more Ti-rich than the lamellar ilmenite (Table 2,

260 an. 11) in the macro-grains of magnetite (Table 2, an. 10)

261

262   DISCUSSION

263   ***1. Crystallographic- and shape-orientation relationships***

264   Regular crystallographic and shape orientation relationships were documented

265 between rock-forming clinopyroxene and the amphibole lamellae it contains as well as among

266 all phases present in the Fe-Ti oxide micro-inclusions and their clinopyroxene hosts (Fig. 4 a,

267 Fig. 5, Fig. 6).

268

269   *1.1. Amphiboles*

270   The lamellar hornblende and actinolite have similar crystallographic orientation

271 relationships to their clinopyroxene host (Fig. 5, Fig. 6), which most likely reflect the

272 geometric (angular) correspondence between the amphibole and clinopyroxene crystal

273 structures (Table 1, Appendix 1). In contrast, the shape orientations of the hornblende and the

274 actinolite lamellae are different (Fig. 1b) and probably reflect a different formation

275 mechanism. The orientation of the hornblende lamellae parallel to the (010) plane and

276 perpendicular to the "b" axis of clinopyroxene minimizes the lattice misfit, because the largest

277 difference in lattice dimensions between clinopyroxene and amphibole occurs along the "b"

278 axis (Table 1, Appendix 1). The (010)-orientation of hornblende in clinopyroxene is

279 preferentially selected during exsolution (Smith, 1977; Yamaguchi et al., 1978) and may be

280 taken as an indication for an exsolution origin of the hornblende lamellae. In contrast, the

281 shape orientation of the actinolite lamellae parallel to the (100) plane of the clinopyroxene

282 does not appear to be controlled by lattice fit. It is rather related to the cracks of parting,

283 where clinopyroxene breaks along planes of structural weakness or along twin planes. Such

284 parting cracks may provide access for fluids allowing hydration and fluid mediated alteration

285 of pyroxene (Yamaguchi et al., 1978), which is in line with the inferred hydrothermal origin

286 of the actinolite lamellae.

287

288   *1.2. Fe-Ti oxide micro-inclusions*

289   For both the X- and Z- type inclusions one of the (110) planes of magnetite is

290 parallel to the (010) plane of the clinopyroxene host (Table 1). However, the X- and Z-type

291 inclusions show different orientation relations to the host mineral in all other crystallographic

292 directions, which corresponds to an about 7° rotation of the X- and Z-type magnetite crystal

293 lattices with respect to one another around their common [110] direction, which is parallel to

294 the "b" axis of the clinopyroxene host (Fig. 4 a). In such mutual orientation, one of the {111}

295 planes of magnetite of the X-type inclusions is parallel to the (-101) plane of the

296 clinopyroxene host, and one of the {111} planes of magnetite of the Z-type inclusions is

297 parallel to the (100) plane of the clinopyroxene host. These planes are important in the context

298 of some similarity between the clinopyroxene and magnetite crystal structures. In

299 clinopyroxene, densely packed oxygen layers occur parallel to both the (-101)- and the (100)-

300 planes, and the {111} planes of magnetite are densely packed oxygen layers as well. Thus,

301 parallel alignment of densely packed oxygen layers is supposedly the prime control on the

302 crystallographic orientation relationships between the studied Fe-Ti oxide micro-inclusions of

303 both the X- and Z-types and their clinopyroxene hosts. This is in line with the findings of

304 Fleet at al. (1980), who infer that the densely packed oxygen layers provide the link between

305 the crystal structures of the inclusion and host phases.

306   Despite of their consistent crystallographic orientations, the elongation directions of

307 the X- and Z-type inclusions are defined by inclusion-host interfaces that follow "irrational"

308 planes in the lattices of both phases. The inclusion-host interfaces neither show accordance

309 with low indexed lattice planes of the magnetite nor of the clinopyroxene. Moreover, the

310 shape orientations of the X- and Z-type inclusions differ by as much as 106° to 107° (Fig. 4

311 b), while the crystallographic orientations only differ by 7° (Fig. 4 a). This phenomenon was

312 first described by Bown and Gay (1959) and since then has been found by several authors

313 (Okamura et al., 1976; Harlow and Klimentidis, 1980; Fleet et al., 1980; Woensdregt et al.,

314 1983; Doukhan et al., 1990; Renne et al., 2002; Feinberg, et al., 2004; Hwang et al., 2010).

315 Fleet et al. (1980) applied the "Optimal phase boundary theory" of Bollmann and Nissen

316 (1968) and suggested that the phase boundaries between the magnetite inclusions and

317 clinopyroxene host that follow "irrational" planes in both lattices are determined by the best

318 geometrical fit between the two crystal lattices at the interface. A detailed discussion of the

319 theory is presented in the Appendix 2. Figure 1 (Appendix 2) is drawn for the best

320 geometrical fit between $(111)_{mt}$ and $(100)_{cpx}$ in the X-type inclusions and between $(-1-11)_{mt}$

321 and $(-101)_{cpx}$ in the Z-type inclusions as is indicated by our EBSD data.

322   The orientation of the optimal magnetite-clinopyroxene phase boundary can be

323 calculated using the equations of Robinson et al. (1977). Combined with thermal expansion

324 coefficients for both magnetite and clinopyroxene, the orientation of the optimum magnetite-

325 clinopyroxene phase boundary was calculated for temperatures from 0 to 1000°C (Fleet et al.,

326 1980, Doukhan et al., 1990, Feinberg et al., 2004). Based on the temperature dependence of

327 the calculated interface orientation, the angle between the elongations of the X- and Z-type

328 inclusions and the angle between Z-type inclusions and the [001] direction of clinopyroxene

329 can be used as a thermometer for magnetite exsolution in clinopyroxene.

330

331   *2. Temperatures of inclusions formation*

332   Referring to the "X-Z-angle - Temperature" diagram of Feinberg et al. (2004) the

333 observed angle between the sets of X- and Z-type inclusions of 106,5° indicates that the

334 exsolution of magnetite from clinopyroxene occurred at a temperature in the range of 800 -

335 900°C, thereby suggesting that the inclusions were formed during cooling of either the early-

336   or late-magmatic clinopyroxene. The spatial association of the magnetite X- and Z-type

337   inclusions with titanian pargasite lamellae and the chemical alteration of the clinopyroxene

338   host in the domains close to the titanian pargasite lamellae, with a composition shift towards

339   the composition of late magmatic clinopyroxene Cpx_2 (according to Pertsev et al., 2015),

340   suggests that the X- and Z-type inclusions were formed during the late magmatic stage of

341   gabbro-41. Application of the amphibole-plagioclase geothermometer of Holland and Blundy

342   (1994) on the compositions of coexisting titanian pargasite and plagioclase yielded

343   temperatures of 830-930° (Pertsev et al., 2015), in line with our estimate from the orientation

344   relations between the X- and Z- type inclusions.

345

346   ***3. Formation mechanisms of the Fe-Ti oxide micro-inclusions***

347   *3.1. X- and Z- types micro-inclusions*

348   The close spatial association of the Fe-Ti oxide inclusions with the (010) oriented

349   amphibole lamellae in clinopyroxene suggests their genetic relation. Lamellar intergrowth of

350   pyroxene and amphibole has been described earlier. Amphibole lamellae parallel to the (010)

351   plane of the clinopyroxene host were interpreted as a result of exsolution, implying the

352   existence of a solid-solution between amphibole and clinopyroxene (Smith, 1977; Yamaguchi

353   et al., 1978). The existence of a solid-solution between amphibole and orthopyroxene has

354   been similarly suggested by Desnoyers (1975). Coupled precipitation of (010) oriented

355   lamellae of tremolitic amphibole and magnetite inclusions in metamorphic diopside was

356   explained by a balanced reaction that involves hydrogen as reactant (Doukhan et al., 1990;

357   Feinberg et al. 2004).

358   Okamura et al. (1976) described orthopyroxenes containing clinopyroxene lamellae

359   and spinel inclusions. They suggested an exsolution mechanism, where during cooling of an

360   originally non-stoichiometric pyroxene the oxygen framework remains intact, while excess Al

361   cations become increasingly unstable on interstitial and tetrahedral sites and migrate to

362   octahedral sites producing domains with spinel-like substructure. Eventually such domains

363   may reach the critical size for producing stable nuclei and lead to the subsequent growth of

364   spinel. According to Okamura et al. (1976) the passive enrichment of Ca in orthopyroxene

365   next to the growth front of the Ca-free spinel and the originally Ca-bearing orthopyroxene

366   resulted in the formation of clinopyroxene lamellae.

367   The mechanism suggested by Okamura et al. (1976) may also be applied to the

368   formation of the X- and Z-type Fe-Ti oxide inclusions and the associated hornblende lamellae

369   in the clinopyroxene of gabbro-41. In the inclusion-bearing domains, the clinopyroxene host

370   is enriched in Ca, Mg and Si and depleted in Al, Ti and Na relative to the inclusion-free

371   domains. These differences reflect the local re-distribution of Al, Ti, Mn, and K into the

372   hornblende lamellae (Fig. 7) that show titanian pargasite composition typical of magmatic

373   amphibole in oceanic gabbro (e.g., Tribuzio et al., 2000; Coogan et al., 2001). We suggest that

374   the iron accumulation in evolved residual liquid during the late-magmatic stage led to the

375   incorporation of Fe into the lattice of the previously formed clinopyroxene (Cpx_1). During

376   cooling, precipitation of the excess Fe according to the mechanism suggested by Okamura et

377   al. (1976) resulted in the formation of the magnetite inclusions. During the partial replacement

378   of the clinopyroxene host by magnetite, Ca, Mg and Si were liberated. These components

379   cannot be accommodated in the magnetite structure, and were re-deposited in the remaining

380   clinopyroxene domains along the phase boundaries. This produced an enrichment of the

381   clinopyroxene in Ca, Mg and Si and a concomitant passive depletion of Al, Ti and Na, which

382   share the same crystallographic sites in clinopyroxene. The decrease of the Al, Ti and Na

383   contents and concomitant increase of Ca and Mg in the octahedral "M1" and "M2" sites and

384   of Si in the tetrahedral "T" site in the late-magmatic clinopyroxene (Cpx_2) calculated based on

385   Morimoto (1988) is shown (Table 2). Re-deposition of Al, Ti, and Na (with H_2O addition

386   from the late-magmatic liquid) in turn resulted in the formation of titanian pargasite. This

387   model is corroborated by the observation that the titanian pargasite lamellae reach their

15

388   maximum thickness in the vicinity of the Fe-Ti oxide micro-inclusions and taper out away

389   from the inclusions. Alternative mechanisms that suggest exsolution of an amphibole-

390   clinopyroxene solid-solution accompanied by substitution of certain oxygen positions by

391   hydroxyl and partial substitution of Ca^{2+} by Na^+ and of Si^{4+} by Al^{3+} (Yamaguchi et al., 1978)

392   cannot explain the observed association of the hornblende lamellae with the Fe-Ti oxide

393   micro-inclusions.

394   Fe-Ti oxide macro-grains crystallized from iron-titanium rich interstitial melt,

395   whereas titanian hornblende seems to form at the same late magmatic stage by interaction

396   between gabbro crystal aggregate and magmatic aqueous fluid, as was proposed by Pertsev et

397   al. (2015) based on the Zr abundances in clinopyroxene and plagioclase compositional trends.

398   Since the evolved iron-titanium rich melt and magmatic aqueous fluid appeared to be in

399   equilibrium, the regular association of compositionally similar titanian hornblende and

400   titanomagnetite micro-inclusions seems to be a micron-scale manifestation of the same late

401   magmatic process. Consequently the appearance of Fe-Ti oxide micro-inclusions associated

402   with (010) titanian hornblende lamellae may indicate a definite type of late magmatic gabbro

403   evolution.

404

405   *3.2. Ilmenite micro-inclusion*

406   Formation of the ilmenite plates in the actinolite lamellae may be attributed to a late

407   hydrothermal alteration process. The actinolite lamellae are oriented parallel to the (100)

408   plane, which is one of the major parting planes of the clinopyroxene host (Fig. 1 c; Fig. 2 b, c;

409   Fig. 7 b). Formation of the actinolite lamellae was likely mediated by access of hydrothermal

410   fluids along these weak zones. Since the high-field strength element Ti is hardly mobile in

411   hydrothermal solutions (Antignano and Manning, 2008) the Ti originally contained in

412   clinopyroxene (up to 1.1 wt.% TiO_2, according to Pertsev et al., 2015) was precipitated

413   directly in place in the form of ilmenite during the replacement of clinopyroxene by actinolite.

414   Probably the patches with hornblende composition within the actinolite lamellae

415   (Table 2, an. 7) reflect an earlier and higher-temperature hydrothermal hornblende being

416   developed along the same (100) parting planes in clinopyroxene. Such a hydrothermal event

417   with the formation of ferropargasite 'Hbl$_3$' (Table 2, an. 8) at about 560-640°C was suggested

418   by Pertsev et al. (2015). Formation of the actinolite-hosted ilmenite plates can thus be

419   explained by re-deposition of the Ti that was liberated during the replacement of the Ti-

420   bearing clinopyroxene or a Ti-bearing precursor amphibole by actinolite in the form of

421   ilmenite.

422   The actinolite-hosted ilmenite plates show crystallographic orientation relationships

423   corresponding to those of the Z-inclusions with the densely packed oxygen layers in the (001)

424   planes of ilmenite aligned with the densely packed oxygen layers parallel to the (100) planes

425   of the actinolite host (Table 1). The observed spatial association of the Z-inclusions and

426   ilmenite plates (Fig. 3 b) may indicate that the Z-inclusions provided nucleation sites for the

427   formation of the actinolite-hosted ilmenite plates.

428   Despite of the fact that the formation of the (100)-oriented actinolite lamellae is

429   attributed to late-stage hydrothermal alteration, the same (100) parting planes may have

430   provided access for aqueous magmatic fluid, which was not in equilibrium with the early-

431   magmatic clinopyroxene, already during the late-magmatic stage. This may explain the

432   observed large-scale distribution of the Z-type inclusions along the (100) clinopyroxene

433   planes and their spatial association with the actinolite lamellae (Fig. 3 b, Fig. 5). The X-type

434   inclusions seem to form in addition to the Z- type inclusions in areas, where the

435   clinopyroxene host underwent particularly intensive iron enrichment such as in the immediate

436   vicinity of big interstitial grains of late magmatic Fe-Ti oxides (Fig. 1a).

437

438   *3.3. Fe-Ti oxide phase content evolution*

439   The exceedingly small size and preferred orientation of the X- and Z-type micro-

440   inclusions hampered the determination of mineral compositions and of the spatial distribution

441   of ulvospinel and/or ilmenite within the magnetite grains. It was thus not possible to infer the

442   evolution of redox state from the compositions of coexisting Fe-Ti oxide phases. According to

443   O'Neill and Navrotsky, (1984) and Wechsler et al., (1984) the temperature of magnetite-

444   ulvospinel unmixing depends on fO_2, cooling rate and the Ti content in the original

445   homogeneous titano-magnetite and is always lower than 600°C. Based on the crystallographic

446   orientation relations, the morphology of the phase intergrowth within the individual

447   multiphase Fe-Ti oxide micro-inclusions and the position of the multiphase Fe-Ti oxide

448   micro-inclusions within the clinopyroxene host we suggest that at the high temperature of the

449   late magmatic stage some Ti was dissolved in the primary late-magmatic magnetite

450   precipitates. During post-magmatic cooling, the Ti-bearing magnetite decomposed into an

451   oriented magnetite-ulvospinel intergrowth (Fig. 2 b) with straight, supposedly coherent phase

452   boundaries between the intergrown phases. The boundaries occur along the {100} planes of

453   both minerals, which is consistent with magnetite-ulvospinel exsolution microstructures

454   (Price, 1980, Feinberg et al., 2005).

455   In the ilmenite-magnetite composite inclusions, ilmenite and magnetite show CORs

456   with $(111)_{mt}$ parallel to $(001)_{ilm}$ and $(110)_{mt}$ parallel to $(100)_{ilm}$, but have uneven phase

457   boundaries (Fig. 2 c, Fig. 5). Their spatial distribution is generally controlled by contacts of

458   the micro-inclusions with the clinopyroxene hosted actinolite lamellae (Fig. 5). In the vicinity

459   of pronounced parting planes the ilmenite and magnetite grains appear strongly corroded (Fig.

460   2 c). Hence, hydrothermal alteration is probably responsible for the appearance of ilmenite in

461   the X- and Z-type composite inclusions. As shown above, the CORs of the homogeneous

462   ilmenite plates were inherited from adjoined Z-type inclusions and may indicate hydrothermal

463   recrystallization of the ilmenite phase of the Z-type inclusions, which was linked to the re-

464   deposition of Ti in sites, where the Ti-bearing clinopyroxene host was replaced by Ti-free

465   actinolite.

466

467   CONCLUSIONS

468   Strong crystallographic orientation relationships (CORs) among Fe-Ti oxide micro-

469   inclusions, associated lamellar amphiboles, and rock-forming clinopyroxene host were

470   established using the EBSD technique. The CORs are determined by the similarity of lattice

471   geometry for the intergrowth of the monoclinic clinopyroxene and amphibole, and by the

472   parallel alignment of close-packed oxygen layers of the Fe-Ti oxide micro-inclusions and the

473   clinopyroxene host. The differences in shape orientations between the (010)-oriented titanian

474   pargasite and the (100)-oriented actinolite lamellae in clinopyroxene are attributed to

475   formation by exsolution and by hydrothermal alteration, respectively.

476   Based on phase content, orientation relationships and associated lamellar amphibole,

477   two genetic types of micro-inclusions were distinguished. A first generation of Fe-Ti oxide

478   micro-inclusions is represented by needle-shaped inclusions represented by intergrowth of

479   magnetite and ilmenite or/and ulvospinel associated with fine lamellae of titanian pargasite.

480   Both the micro-inclusions and hornblende are oriented parallel to the (010) plane of the

481   clinopyroxene host and are attributed to an exsolution reaction, which lead to the

482   redistribution of excess Fe and distinct behavior of major and minor elements in non-

483   stoichiometric late-magmatic clinopyroxene during cooling. The needle-shaped Fe-Ti oxide

484   micro-inclusions show two distinct elongation directions, with the group of more abundant Z-

485   type inclusions showing elongation sub-parallel to the [001] direction of the clinopyroxene

486   host and the group of less abundant X-type inclusions showing elongation sub-parallel to the

487   [100] direction of the clinopyroxene host. The observed elongation directions imply

488   inclusion-host interfaces that follow "irrational" planes of both the minerals.

489   Based on the optimal phase boundary geothermometer the angle between the

490   elongation directions of the two sets of needle-shaped micro-inclusions indicates an

491   exsolution temperature of 800-900°C confirming their attribution to the late-magmatic stage.

492   The formation of the Fe-Ti oxide inclusions and of the titanian pargasite lamellae was

493   probably related to the same process involving introduction of Fe via a late magmatic fluid or

494   melt, and micro-scale intra-crystalline re-distribution of components, which determines the

495   specific chemical composition of the late-magmatic hornblende and clinopyroxene. A second

496   generation of Fe-Ti oxide micro-inclusions is represented by plate-shaped homogenous

497   ilmenite within actinolite lamellae, which are attributed to a hydrothermal process. The

498   ilmenite is considered to be the result of the re-deposition of Ti during hydrothermal

499   replacement of the late magmatic Ti-bearing clinopyroxene or high-temperature lamellar

500   hornblende by actinolite along the (100) parting planes of the clinopyroxene host.

501   Clinopyroxene-hosted Fe-Ti oxide micro-inclusions associated with lamellar

502   amphiboles can serve as reliable indicators of major petrogenetic events in the host rock

503   history. Our example (gabbro-41) shows that Fe-Ti oxide micro-inclusions formed as a result

504   of chemical alteration and phase transformations of primary rock-forming minerals indicating

505   late-magmatic and hydrothermal processes. The evolution of the silicate-hosted Fe-Ti oxide

506   micro-inclusions seems useful to constrain the provenance of different gabbro assemblages

507   from modern oceanic crust and ophiolites.

508

515

516

REFERENCES

Agar, S. M., and G. E. Lloyd (1997), Deformation of Fe-Ti oxides in gabbroic shear zones from the MARK area, Proc. Ocean Drill. Program Sci. Results, 153, 123–135.

Ageeva, O., Habler, G., Topa, D., Waitz, T., Li, C., Pertsev, A., . Thomas Griffiths, T., Zhilicheva, O,. & Abart, R. (2016). Plagioclase hosted Fe-Ti-oxide micro-inclusions in an oceanic gabbro-plagiogranite association from the Mid Atlantic ridge at 13° 34'N. American Journal of Science, 316(2), 85-109.

Antignano, A., & Manning, C. E. (2008). Rutile solubility in H_2O, H_2O–SiO_2, and H_2O–$NaAlSi_3O_8$ fluids at 0.7–2.0 GPa and 700–1000 C: implications for mobility of nominally insoluble elements. *Chemical Geology*, *255*(1), 283-293.

Amburstmacher, T. J., and Banks, N. G., 1974, Clouded plagioclase in metadolerite dikes, southeastern Bighorn Mountains, Wyoming: American Mineralogist, v. 59(7-8), p. 656-665.

Armbrustmacher, T. J., and Banks, N. G., 1974, Clouded plagioclase in metadolerite dikes, southeastern Bighorn Mountains, Wyoming: American Mineralogist, v. 59(7-8), p. 656-665.

Auzende, J.-M., Bideau, D., Bonatti, E., Cannat, M., Honnorez, J., Lagabrielle, Y., Malavieille, J., Mamaloukas-Frangoulis, V. and Mevel, C. (1989). Direct observation of a section through slow-spreading oceanic crust. Nature 337, 726–729.

Bollmann, W. T., and Nissen, H. U. (1968). A study of optimal phase boundaries: the case of exsolved alkali feldspars. Acta Crystallographica Section A: Crystal Physics, Diffraction, Theoretical and General Crystallography, 24(5), 546-557.

Bonatti, E., Ligi, M., Brunelli, D., Cipriani, A., Fabretti, P., Ferrante, V., Gasperini, L. and Ottolini, L. (2003). Mantle thermal pulses below the Mid-Atlantic Ridge and temporal variations in the formation of oceanic lithosphere. Nature 423, 499–505.

Bonatti, E., Brunelli, D., Buck, W. R., Cipriani, A., Fabretti, P., Ferrante, V., Gasperini, L. and Ligi, M. (2005). Flexural uplift of a lithospheric slab near the Vema Transform (Central Atlantic): Timing and Mechanisms. Earth and Planetary Science Letters 240, 642–655.

548   Bown, M. G., and P. Gay. "The identification of oriented inclusions in pyroxene crystals."
549   American Mineralogist 44.5-6 (1959): 592-602.

550   Cipriani, A., Bonatti, E., Brunelli, D. and Ligi, M., 2009. 26 million years of mantle
551   upwelling below a segment of the Mid Atlantic Ridge: The Vema Lithospheric
552   Section revisited. Earth and Planetary Science Letters, 285(1), pp.87-95.

553   Coogan, L. A., Wilson, R. N., Gillis, K. M. & MacLeod, C. J. (2001). Near-solidus evolution
554   of oceanic gabbros: Insights from amphibole geochemistry. Geochimica et
555   Cosmochimica Acta 65, 4339–4357.

556   Davis, K. E. (1981). Magnetite rods in plagioclase as the primary carrier of stable NRM in
557   ocean floor gabbros. Earth and Planetary Science Letters, 55(1), 190-198.

558   Dégi, J., Abart, R., Török, K., Rhede, D., and Petrishcheva, E., 2009, Evidence for xenolith–
559   host basalt interaction from chemical patterns in Fe–Ti-oxides from mafic
560   granulite xenoliths of the Bakony–Balaton Volcanic field (W-Hungary):
561   Mineralogy and Petrology, v. 95(3-4), p. 219-234.

562   Desnoyers, C. Exsolutions d'amphibole, de grenat et de spinelle dans les pyroxenes de roches
563   ultrabasiques: peridotite et pyroxenolites. Bull. Soc. Franc. Mineral. Crist. 98,
564   65-77 (1975)

565   Dick, H.J.B., Natland,J.H., Alt, J.C., Bach, W., Bideau, D., Gee, J.S., Haggas, S., Hertogen,
566   J.G.H., Hirth, G., Holm, P.M., Ildefonse, B., Iturrino, G.J., John, B.E., Kelley,
567   D.S., Kikawa, E., Kingdon, A., LeRoux, P.J., Maeda, J., Meyer, P.S., Miller,
568   D.J., Naslund, H.R., Niu, Y.-L., Robinson, P.T., Snow, J., Stephen, R.A.,
569   Trimby, P.W., Worm, H.-U., Yoshinobu, A., 2000. A Long In-Situ Section of
570   the Lower Ocean Crust: Results of ODP Leg 176 Drilling at the Southwest
571   Indian Ridge. Earth and Planetary Sciences 179, 31-51

572   Divljan, S., 1960, The results of field and laboratory studies of aventurine plagioclases from
573   some Norwegian pegmatites: Proceedings of the 21st International Geological
574   Congress, Norden, v. 17, p. 94-101.

575   Doukhan, N., Ingrin, J., Doukhan, J. C., & Latrous, K. (1990). Coprecipitation of magnetite
576   and amphibole in black star diopside; a TEM study. American Mineralogist,
577   75(7-8), 840-846.

578   Feinberg, J. M., Wenk, H. R., Renne, P. R., & Scott, G. R. (2004). Epitaxial relationships of
579   clinopyroxene-hosted magnetite determined using electron backscatter
580   diffraction (EBSD) technique. American Mineralogist, 89(2-3), 462-466.

581   Feinberg, J. M., Scott, G. R., Renne, P. R., & Wenk, H. R. (2005). Exsolved magnetite
582   inclusions in silicates: Features determining their remanence behavior.
583   Geology, 33(6), 513-516.

584   Fleet, Michael E., Gregory A. Bilcox, and Robert L. Barnett. "Oriented magnetite inclusions
585   in pyroxenes from the Grenville Province." Canadian Mineralogist 18.1
586   (1980): 89-99.

587   Grimes, C.B., John, B.E., Cheadle, M.J. and Wooden, J.L., 2008. Protracted construction of
588   gabbroic crust at a slow spreading ridge: Constraints from 206Pb/238U zircon
589   ages from Atlantis Massif and IODP Hole U1309D (30 N, MAR).
590   Geochemistry, Geophysics, Geosystems, 9(8).

591   Hargraves, R. B., and Young, W. M., 1969, Source of stable remanent magnetism in
592   Lambertville diabase: American Journal of Science, v. 267, n. 10, p. 1161–
593   1177

594   Harrison, R.J., Dunin-Borkowski, R.E., and Putnis, A., 2002, Direct imaging of nanoscale
595   magnetic interactions in minerals: National Academy of Sciences Proceedings,
596   v. 99, p. 16,556–16,561.

597   Harlow, G. E., and R. Klimentidis. "Clouding of Pyroxenes and Plagioclases in Eucrites:
598   Implications for Post-Crystallization Processing."Lunar and Planetary Science
599   Conference. Vol. 11. 1980.

600   Hayman, N.W., Grindlay, N.R., Perfit, M.R., Mann, P., Leroy, S. and de Lépinay, B.M.,
601   2011. Oceanic core complex development at the ultraslow spreading Mid-
602   Cayman Spreading Center. Geochemistry, Geophysics, Geosystems, 12(3).

603   Hekinian, R., 2014. Sea Floor Rocks. In Sea Floor Exploration (pp. 75-108). Springer
604   International Publishing.

605   Holland, T.J.B., and Blundy, J.D. (1994) Non-ideal interactions in calcic amphiboles and
606   their bearing on amphibole-plagioclase thermometry. Contributions to
607   Mineralogy and Petrology, 116, 433–447.

608   Hwang, S.-L., Shen, P., Yui, T.-F. & Chu, H.-T. (2010). On the coherency-controlled growth
609   habit of precipitates in minerals. J. Appl. Cryst. 43, 417–428.

610   Jaffe, H. W., Robinson, Peter and Tracy, R. J. (1975) Orientation of pigeonite exsolution
611   lamellae in metamorphic augite: correlation with composition and calculated
612   optimal phase boundaries. American Mineralogist, 60, 9-28

613   Leake, B. E., Woolley, A. R., Arps, C. E. S., Birch, W. D., Gilbert, M. C., Grice, J. D.,
614   Hawthorne, F. C., Kato, A., Kisch, H. J., Krivovichev, V. G., Linthout, K.,

615   Laird, J., Maresch, W. V., Nickel, E. H., Schumacher, J. C., Smith, D. C.,

616   Stephenson, N. C. N., Whittaker, E. J. W. & Guo, Y. (1997). Nomenclature of

617   amphiboles of the International Mineralogical Association, Commission on

618   New Minerals and Mineral Names. Canadian Mineralogist 35, 219–246.

619   Malpas, J. and Robinson, P., 1997. OCEANIC LITHOSPHERE 1. The Origin and Evolution

620   of Oceanic Lithosphere: Introduction. Geoscience Canada, 24(2).

621   Morimoto, N. "Nomenclature of pyroxenes." Mineralogy and Petrology 39.1 (1988): 55-76.

622   Neumann H., and Christie, O. H. J., 1962, Observation of plagioclase aventurines from

623   Southern Norway: Norsk Geologisk Tidsskrift, v. 42, no. 2, p. 389-393

624   Natland, J. H., Meyer, P. S., Dick, H. J., & Bloomer, S. H. (1991). Magmatic oxides and

625   sulfides in gabbroic rocks from Hole 735B and the later development of the

626   liquid line of descent. In Von Herzen, RP, Robinson, PT, et al., Proc. ODP,

627   Sci. Results (Vol. 118, pp. 75-111).

628   O'Neill, Hugh St C., and Alexandra Navrotsky. "Cation distributions and thermodynamic

629   properties of binary spinel solid solutions." American Mineralogist 69.7-8

630   (1984): 733-753.

631   Okamura, F. P., McCallum, I. S., Stroh, J. M., & Ghose, S. (1976). Pyroxene-spinel

632   intergrowths in lunar and terrestrial pyroxenes. In Lunar and Planetary Science

633   Conference Proceedings (Vol. 7, pp. 1889-1899).

634   Pertsev, A. N., Aranovich, L. Y., Prokofiev, V. Y., Bortnikov, N. S., Cipriani, A., Simakin, S.

635   S., & Borisovskiy, S. E. (2015). Signatures of Residual Melts, Magmatic and

636   Seawater-Derived Fluids in Oceanic Lower-Crust Gabbro from the Vema

637   Lithospheric Section, Central Atlantic. Journal of Petrology, 56 (6), 1069-

638   1088.

639   Poldervaart, A., and Gilkey, A. K., 1954, On clouded plagioclase. American mineralogist, v.

640   39(1-2), p. 75-91.

641   Pouchou J. L., Pichoir F. Electron Probe Quantitation (KFJ Heinrich, DE Newbury, eds.)

642   //Pleunum, New York. – 1991. – C. 1-75.

643   Price, G.D., 1980, Exsolution microstructures in titano-magnetites and their magnetic

644   significance: Physics of the Earth and Planetary Interiors, v. 23, p. 2–12.

645   Ram, F., Zaefferer, S., Jäpel, T., and Raabe, D. (2015) Error analysis of the crystal

646   orientations and disorientations obtained by the classical electron backscatter

647   diffraction technique. Journal of Applied Crystallography, 48, 797–813.

648   Ramdohr P. Ulvöspinel and its significance in titaniferous iron ores //Economic Geology. –
649   1953. – T. 48. – №. 8. – C. 677-688.

650   Renne, P. R., Scott, G. R., Glen, J. M., & Feinberg, J. M. (2002). Oriented inclusions of
651   magnetite in clinopyroxene: Source of stable remanent magnetization in
652   gabbros of the Messum Complex, Namibia. Geochemistry, Geophysics,
653   Geosystems, 3(12), 1-11.

654   Robinson, P., Jaffe, H. W., Ross, M., & Klein, C. (1971). Orientation of exsolution lamellae
655   in clinopyroxenes and clinoamphiboles: consideration of optimal phase
656   boundaries. American Mineralogist, 56(5-6), 909.

657   Robinson, P., Ross, M., Nord, G.L., Smyth, J.R., and Jaffe, H.W. (1977), Exsolution lamellae
658   in augite and pigeonite: Fossil indicators of lattice parameters at high
659   temperature and pressure. American Mineralogist, 62, 857-873.

660   Sauerzapf, U., Lattard, D., Burchard, M., and Engelmann, R., 2008, The titanomagnetite–
661   ilmenite equilibrium: new experimental data and thermo-oxybarometric
662   application to the crystallization of basic to intermediate rocks: Journal of
663   Petrology, v. 49(6), p. 1161-1185.

664   Smirnov, A. V., Tarduno J. A., and Pisakin B. N., 2003, Paleointensity of the Early
665   Geodynamo (2.45 Ga) as Recorded in Karelia: A Single Crystal Approach:
666   Geology, v. 31, p. 415-418.

667   Smith, J. V., 1974, Feldspar Minerals. Tom 2. Chemical and Textural Properties. Springer-
668   Verlag. 690 p.

669   Smith P. P. K. An electron microscopic study of amphibole lamellae in augite. Contributions
670   to Mineralogy and Petrology. 1977. T. 59. №. 3. C. 317-322.

671   Sobolev, P. O., 1990, Orientation of acicular iron-ore mineral inclusions in plagioclase:
672   International Geology Review, v. 32(6), p. 616-628.

673   Tribuzio, R., Tiepolo, M. & Thirlwall, M. F. (2000). Origin of titanian pargasite in gabbroic
674   rocks from the Northern Apennine ophiolites (Italy): insights into the late-
675   magmatic evolution of a MOR-type intrusive sequence. Earth and Planetary
676   Science Letters 176, 281–293.

677   Usui, Y., Nakamura, N., and Yoshida, T., 2006, Magnetite micro-exsolutions in silicate and
678   magmatic flow fabric of the Goyozan granitoid (NE Japan): Significance of
679   partial remanence anisotropy: Journal of Geophysical Research: Solid Earth
680   (1978–2012), 111(B11). doi: 10.1029/2005JB004183

681 Wechsler, Barry A., Donald H. Lindsley, and Charles T. Prewitt. Crystal structure and cation
682   distribution in titanomagnetites ($Fe_{(3-x)}Ti_xO_4$). American Mineralogist 69.7-8
683   (1984): 754-770.

684 Wenk, H. R., Chen, K., and Smith, R., 2011, Morphology and microstructure of magnetite
685   and ilmenite inclusions in plagioclase from Adirondack anorthositic gneiss:
686   American Mineralogist, v. 96(8-9), p. 1316-1324.

687 Woensdregt, C. F., M. Weibel, and R. Wessicken. "Electron microscopical investigation of
688   oriented magnetite and amphibole in black star diopside." Schweizerische
689   Mineralogische und Petrographische Mitteilungen 63.2-3 (1983): 167-176.

690 Xu, W., Geissman, J. W., Van der Voo, R., & Peacor, D. R. (1997). Electron microscopy of
691   iron oxides and implications for the origin of magnetizations and rock
692   magnetic properties of Banded Series rocks of the Stillwater Complex,
693   Montana. Journal of Geophysical Research: Solid Earth, 102(B6), 12139-
694   12157.

695 Yamaguchi, Yoshiaki, Junji Akai, and Katsutoshi Tomita. Clinoamphibole lamellae in
696   diopside of garnet lherzolite from Alpe Arami, Bellinzona, Switzerland.
697   Contributions to Mineralogy and Petrology 66.3 (1978): 263-270.

698

699

700

701 **APPENDIX 1**

702   METHODS

703   *Electron Backscatter Diffraction Analysis*

704   A mechanically and chemo-mechanically polished carbon-coated thin section was

705 used for Electron Back-Scatter Diffraction (EBSD) analysis. EBSD measurements were

706 performed at the Laboratory for Scanning Electron Microscopy and Focused Ion Beam

707 Applications (Faculty of Geosciences, Geography and Astronomy) at the University of

708 Vienna (Austria) using an FEI Quanta 3D FEG instrument. This FIB-SEM is equipped with a

709 Field Emission Electron Source (Schottky-Emitter) and a Digiview IV EBSD camera, which

710 is mounted at 0° azimuth and 5° elevation angle. Electron beam settings during EBSD data

711   collection were at 15kV accelerating voltage and approximately 4nA probe current (in

712   analytic electron beam mode), while the sample was positioned at 14 mm working distance

713   and at 70° tilted surface leading to a 20° beam incidence angle. The pattern center calibration

714   was carefully fine-tuned based on an excellent pattern taken at a position in the center of the

715   FSE image. The EDAX OIM Data Collection Software versions 6.2 and 7.3 were used for

716   EBSD data collection. Crystallographic orientation maps were processed by EDAX OIM

717   Analysis version 7.3, whereas the single point data were processed using the MTEX toolbox

718   for Matlab (version 4.1.4).

719   A total of 72 single point analyses (17 magnetite/ulvospinel, 36 ilmenite, 16

720   diopside, 3 amphibole data points) were collected manually using a 2x2 binning of the EBSD

721   camera resolution. Each indexing result was optimized by adjusting the Hough settings. The

722   Rho-fraction, minimum Hough peak intensity, minimum peak distance in Hough space as

723   well as the maximum and minimum number of bands used for indexing were varied for each

724   measurement in order to optimize the indexing statistics. The reference structure files listed in

725   Table 1 (Appendix 1), were used for indexing EBSD patterns. Ilmenite showed significant

726   pseudosymmetric misindexing when using the correct reference structure file with trigonal

727   rhombohedral symmetry (H-M Symbol -3). In order to eliminate misindexing, the interplanar

728   angle tolerance was set to 2° and the EBSD band-width additionally was considered when

729   indexing ilmenite. For indexing all other phases only the band center position in the EBSD

730   pattern was used disregarding the band width. Actinolite and hornblende could not be

731   distinguished solely by crystal structure. The hornblende reference structure was used for

732   indexing hornblende single point data, whereas for mapping, both amphibole phases were

733   indexed using the actinolite reference structure. Resulting orientations from using either

734   amphibole reference structures are identical within the angular resolution of Hough transform

735   based EBSD indexing (Ram et al., 2015).

736   Two crystallographic orientation maps were collected at camera settings of 4x4

737   binning and 64.5 milliseconds exposure time. Hough settings were at a binned pattern size of

738   140x140 pixels, a theta step size of 0.5°, a Rho-fraction of 91%, a minimum peak distance of

739   9 pixels and a 9x9 pixels convolution mask. The number of bands used for indexing ranged

740   from 3 to 15. Map data were collected in hexagonal grid mode at 40 nm step size. In order to

741   increase the fraction of data points with a confidence index value above 0.1, the dataset was

742   cleaned by the confidence index standardization routine and the neighbor orientation

743   correlation method (level 1, i.e. the orientation of data points is changed according to 5

744   identically oriented next-neighbour points). This cleaning procedure leads to 98.8% (scan01)

745   or 90.6 % (scan02) of the data points with a CI value > 0.1 compared to 91.4% (scan01) and

746   62.5% (scan02) of the unprocessed datasets.

747

748   *Universal Stage Measurements*

749   A universal stage was used for determining the shape orientations of the Fe-Ti oxide

750   inclusions and amphibole lamellae with respect to the lattice of the clinopyroxene host, the

751   crystallographic orientation of which had previously been determined using EBSD. For

752   measuring the angular relations between "X"- and "Z"- type inclusions the thin section was

753   positioned so that the (010) plane of the clinopyroxene host was oriented perpendicular to the

754   optical axis of the microscope. In this position the angle between the "X"- and "Z"- type

755   micro-inclusions could be measured directly, because they both lie in the (010) plane of the

756   clinopyroxene host. If only one of the inclusion types was in the field of view, the angle

757   between the long axis of the inclusion and the traces of the $(100)_{cpx}$ parting planes, which in

758   this section are oriented parallel to the microscope optical axis, was determined. The

759   reproducibility of universal stage measurements depended on the size of the inclusions and on

760   the inclination of the (010) plane of the pyroxene host with respect to the thin section surface.

761   Repeated measurements varied from ±0.5° to ±2°. A total of 50 measurements were used to

762   obtain the mean and standard deviation of the angle between the elongation directions of the

763   X- and Z-type inclusions.

764

765   *Electron probe microanalysis (EPMA)*

766   Electron probe microanalyses were performed at the Department of Lithospheric

767   Research, University of Vienna using a Cameca SXFyve electron probe micro analyzer

768   equipped with 5 wavelength- and one energy-dispersive spectrometer. Well-characterized

769   homogeneous natural and synthetic minerals were used as standards. Analyses were done

770   using a focused beam at 15 kV accelerating voltage and 20 nA beam current. Counting times

771   were 20 seconds on the peak position and 10 seconds on each background position. To

772   minimize loss of Na due to vaporization, the beam was defocused to a diameter of 5 microns

773   and 10 seconds counting time on the peak position were used for the analysis of feldspar. The

774   PAP method (Pouchou and Pichoir, 1991) was used for matrix corrections. The relative error

775   of the laboratory internal standard is below 1%.

776

777

778   **APPENDIX 2**

779   THE OPTIMAL PHASE BOUNDARY THEORY APPLICATION

780   The underlying rationale of the optimal phase boundary theory suggested in

781   (Bollmann and Nissen, 1968) is that phase boundaries between a solid phase precipitate and

782   its host preferentially attain orientations that minimize interfacial energy. According to

783   Bollmann and Nissen (1968) the interfacial energy is minimized for interface orientations

784   corresponding to the best geometrical fit between the two crystal lattices at the interface. In

785   their endeavor to explain the shape and crystallographic orientation relations between

786   pigeonite lamellae and an augite host Robinson, et al., (1971, 1977) and Jaffe et al., (1975)

787   showed that for two monoclinic lattices aligned along their common b-direction and having

788   similar "b" parameter perfect coherency between a set of two lattice planes of each of the

789   lattices exists for two specific crystallographic orientation relations, which are related to each

790   other by a rotation about the common "b" axis. The interface with perfect coherency between

791   the two sets of two lattice planes was referred to as "perfect interface" by Robinson, et al.

792   (1971). It has an "irrational" though precisely defined orientation with respect to both lattices.

793   Due to the pressure- and temperature-dependence of the lattice parameters, the orientation of

794   the "perfect interface" changes with pressure and temperature, a property, which has been

795   calibrated as a geothermometer for clinopyroxene-clinopyroxene and clinoamphibole-

796   clinoamphibole lamellar intergrowths (Robinson et al., 1971, 1977; Jaffe et al., 1975).

797   Fleet et al. (1980), Doukhan et al. (1990) and Feinberg et al. (2004) applied the

798   relations derived by Robsinon et al. (1971, 1977) to clinopyroxene hosted magnetite

799   inclusions. Fleet et al. (1980) and later Feinberg et al. (2004) suggested a non-primitive

800   monoclinic cell for magnetite, with the monoclinic diad axis parallel to the [110]-direction of

801   magnetite, and a modified monoclinic cell for clinopyroxene. A projection of the monoclinic

802   cells of magnetite and clinopyroxene down their common "b"-direction is shown in Figure 1

803   (Appendix 2). The figure is drawn for perfect alignment of $(111)_{mt}$ and $(100)_{cpx}$ in the X-type

804   inclusions and perfect alignment of $(-1-11)_{mt}$ and $(-101)_{cpx}$ in the Z-type inclusions as is

805   indicated by our EBSD data. These CORs correspond to a 7° rotation of the two magnetite

806   lattices with respect to one another around their common [110]-direction. It is seen that for Z-

807   type inclusions perfect coherency between the $(-1-11)_{mt}$ and $(-101)_{cpx}$ planes exists along the

808   heavy solid lines that are slightly inclined relative to the clinopyroxene [001]-direction.

809   Similarly, for the X-type inclusions perfect coherency between the $(111)_{mt}$ and $(100)_{cpx}$ planes

810   exists along the heavy solid lines that are slightly inclined relative to the clinopyroxene [100]-

811   direction. It is interesting to note that the spacing between the possible coherent interfaces is

812   significantly lower for the Z-type orientation than for the X-type orientation of the magnetite.

813   The Z-type COR is thus more favorable for producing coherency between densely packed

814 oxygen layers at the inclusion-host interface than the X-type orientation. This may explain

815 that the Z-type inclusions are more commonly observed than the X-type inclusions, which is

816 the case in the present study and was documented in earlier studies (Fleet et al. 1980).

817   "Perfect boundaries" in the sense of Robinsons et al (1971) with coherency of both,

818 the $(111)_{mt}$ - $(100)_{cpx}$ pair as well as the $(-1-11)_{mt}$ and $(-101)_{cpx}$ pairs at the magnetite-

819 clinopyroxene interface would require counterclockwise rotation of the X-type magnetite

820 lattice by about 1.8° and clockwise rotation of the Z-type magnetite lattice by about 0,4°.

821 This would slightly change the orientation and the spacing of possible coherent interfaces but

822 would not change the fact that the spacing between possible coherent interfaces is

823 significantly smaller for Z-type than for the X-type inclusions.

824

825 **LIST OF FIGURES**

a   б
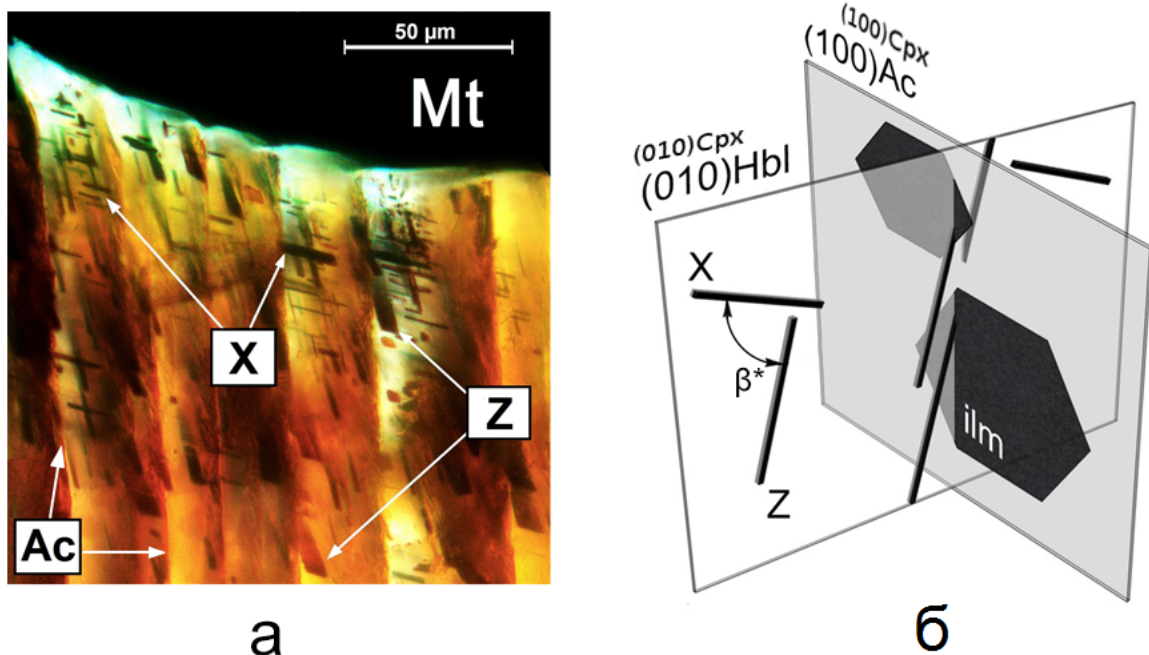
826

827 Figure 1. (a) Transmitted light image of clinopyroxene-hosted X- and Z-type inclusions near a

828 big magnetite grain (Mt). (b) Schematic drawing of a $(010)_{cpx}$ -oriented hornblende lamella

829 comprising X- and Z-type inclusions and of a $(100)_{cpx}$ -oriented actinolite lamella with

830   ilmenite plates. The angle between the X- and Z-type inclusions that is used as a

831   geothermometer is marked β*; Hbl – hornblende, Ac – actinolite, ilm – ilmenite

832
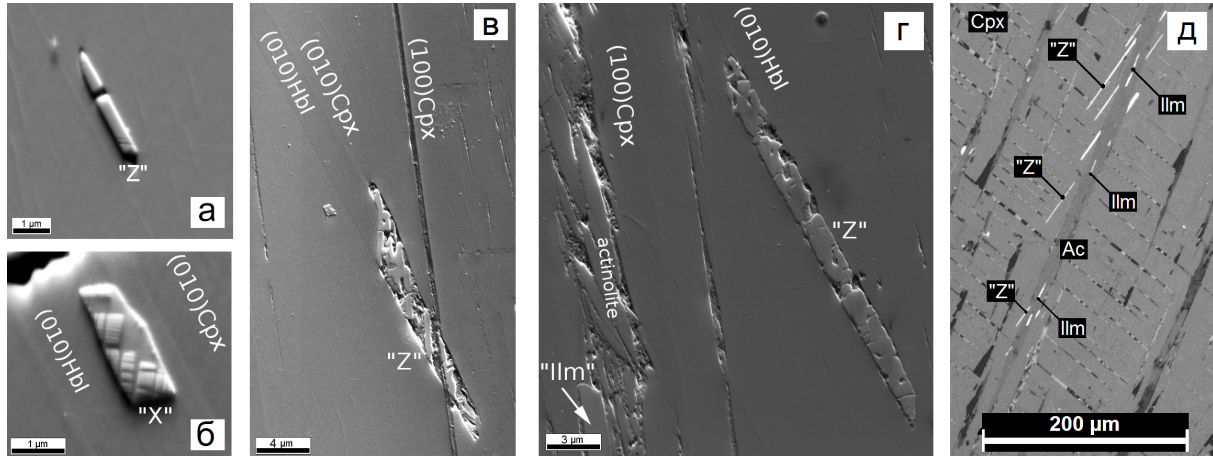
834   Figure 2. Forward-scattered electron (FSE) images (a, b) and secondary electron (SE) image

835   (c) showing X- and Z-type inclusions lying in the (010) plane of clinopyroxene (Cpx): (a)

836   needle-shaped inclusion predominantly composed of magnetite; (b) inclusion represented by

837   magnetite-ulvospinel intergrowth and hornblende (Hbl) lamellae oriented parallel to (010)$_{cpx}$;

838   (c) crack along the (100)$_{cpx}$ parting plane crosscutting an altered inclusion, which follows a

839   hornblende lamella in clinopyroxene.

840
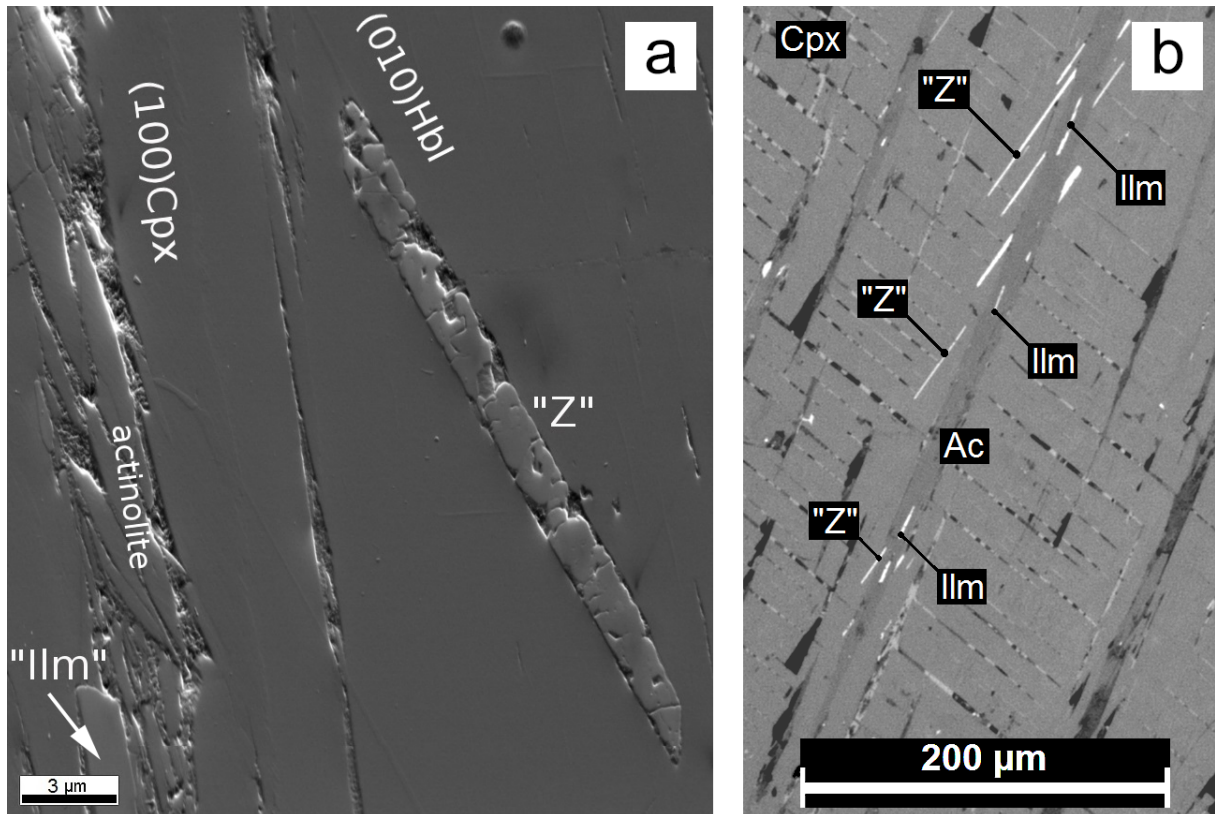
Figure 3. (a) Secondary electron (SE) images of a magnetite-ilmenite Z-type inclusion and an actinolite lamella with ilmenite (Ilm) inclusion; (b) optical reflected light image of ilmenite plates (Ilm) in an actinolite lamella (Ac), and adjoined ilmenite-magnetite Z-type inclusions in the clinopyroxene host. The transversal cracks are oriented sub-parallel to $(001)_{cpx}$, and contain unidentified Fe-oxide or Fe-hydroxide phases, they probably represent altered pigeonite lamellae similar to those described in Robinson at al. (1971).
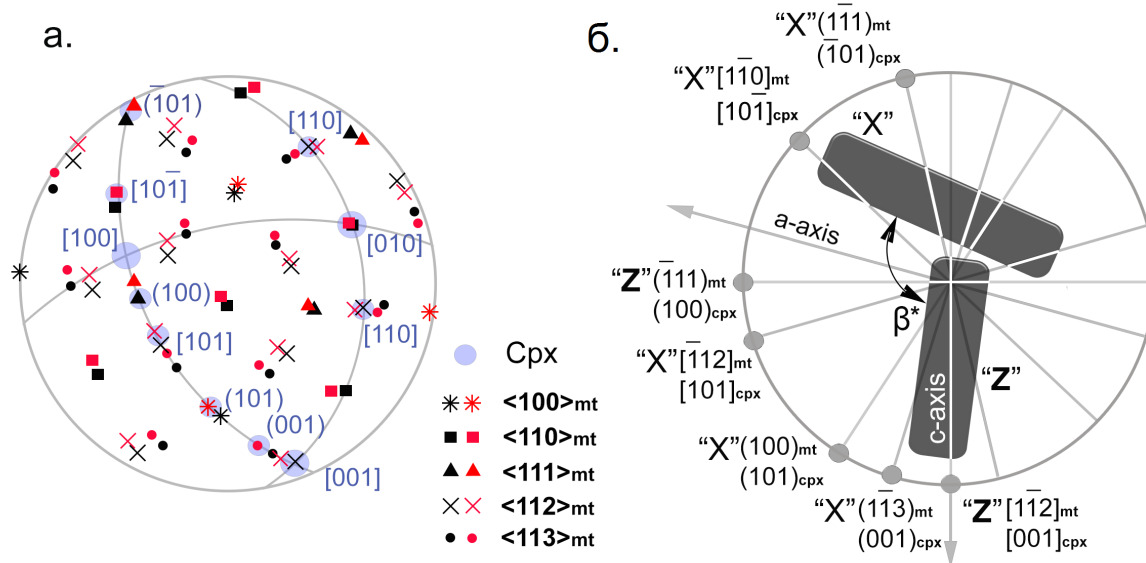
Figure 4. (a) Stereographic projection (upper hemisphere) showing the poles of lattice planes and lattice directions of the clinopyroxene host (blue circles) and magnetite of X-type inclusions (red) and Z-type inclusions (black) as obtained from EBSD analysis; the crystallographic correspondence between X- and Z-type inclusions and the clinopyroxene host is given in Table 1. (b) Crystallographic and shape orientation relations between Fe-Ti oxide micro-inclusions and clinopyroxene host. Projection down the [010] direction of the clinopyroxene host: the long axes of the X- and Z-type inclusions are subparallel to the a- and c- axes of clinopyroxene and corresponding CORs are shown. The angle between the X- and Z-type inclusions that is used as a geothermometer is marked as β^*.
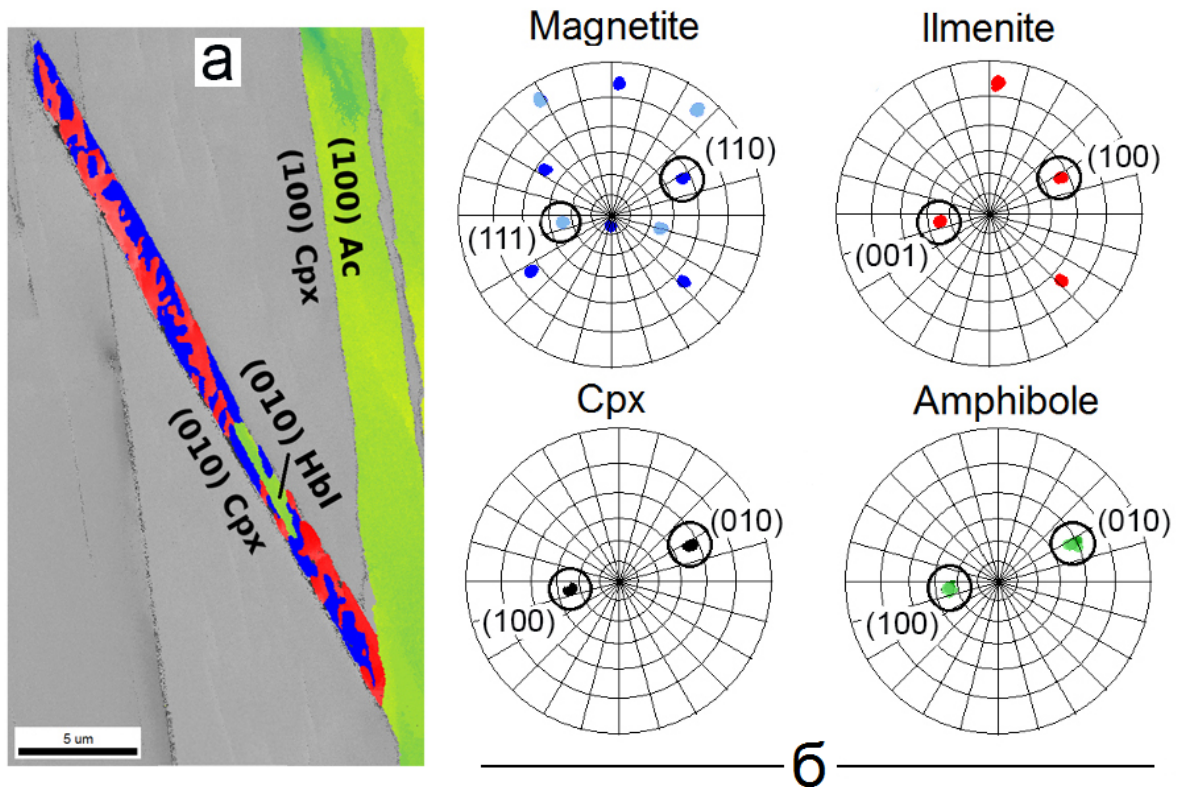
Figure 5. (a) EBSD orientation distribution map of clinopyroxene (gray) hosted composite magnetite (blue) – ilmenite (red) Z-type micro-inclusion and associated amphiboles (green), (010)-hornblende and (100)-actinolite lamellae, the crystallographic planes corresponding to the phase boundary orientations are indicated; (b) pole figures of EBSD orientation data with corresponding lattice elements indicated by open circles;
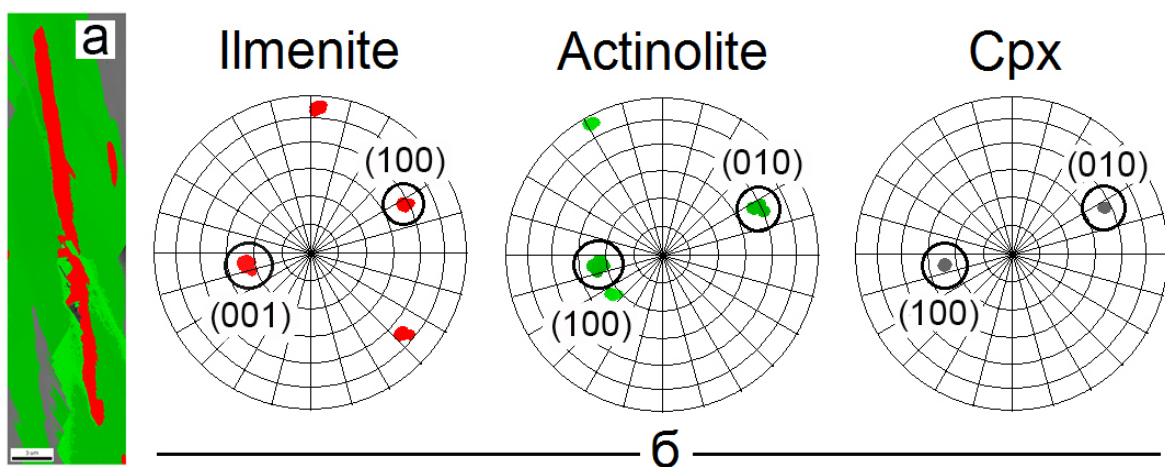
868   Figure 6. (a) Orientation distribution map of ilmenite plates (red) in an actinolite (100)-

869   lamella (green) within clinopyroxene (gray); (b) corresponding pole figures. The deflection of

870   the actinolite from the main orientation is caused by twinning (bright green).
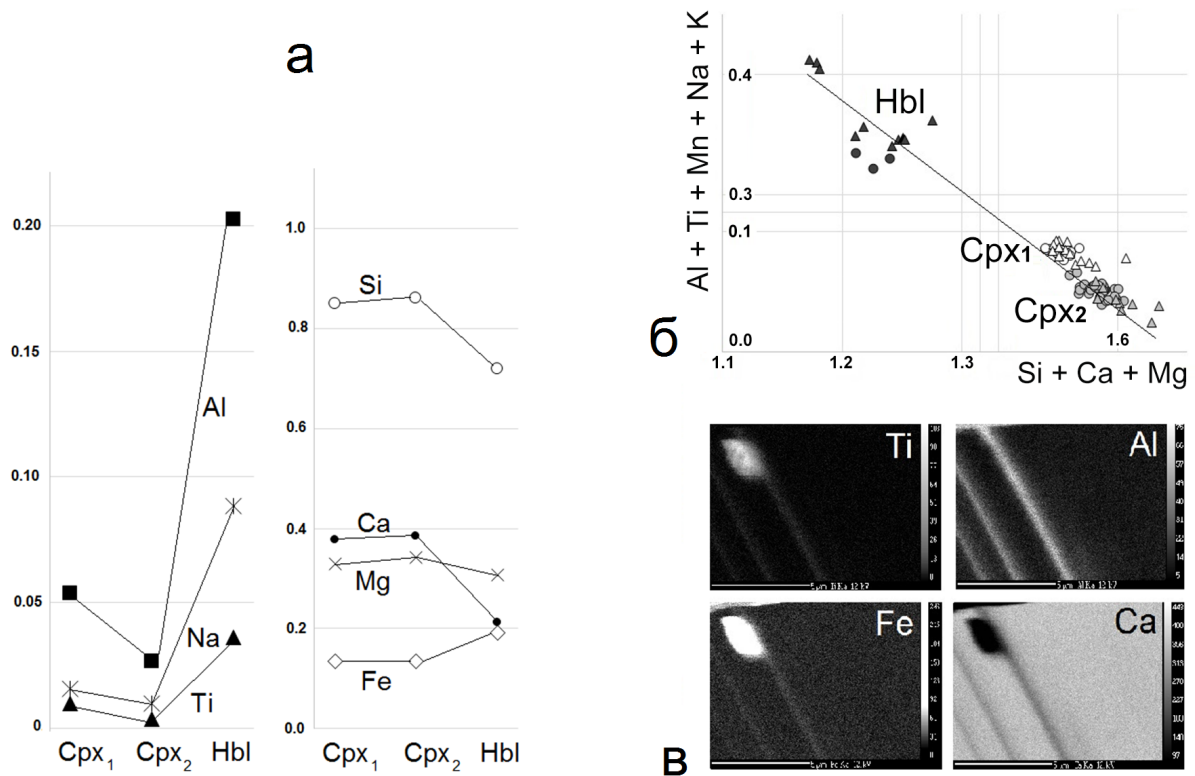

871

872   Figure 7. (a) Composition variation (molar proportions, based on singe analyses) across the

873   transition from Cpx_1 via Cpx_2 to titanian pargasite (Hbl). (b) Al+Ti+Mn+Na+K vs Si+Ca+Mg

874   (molar proportions) in clinopyroxenes and amphibole of gabbro-41 according to our data

875   (circles), and data previously published by Pertsev et al. (2015) (triangles); the clinopyroxenes

876   Cpx_1 and Cpx_2 are marked by white and gray symbols, amphibole Hbl is marked by black

877   symbols; (c) Element map of ulvospinel-magnetite micro-inclusion and associated Hbl

878   lamellae (corresponding to those shown in Figure 2 b) in clinopyroxene.

879

880

881   **FIGURE (Appendix 2)**

882

883
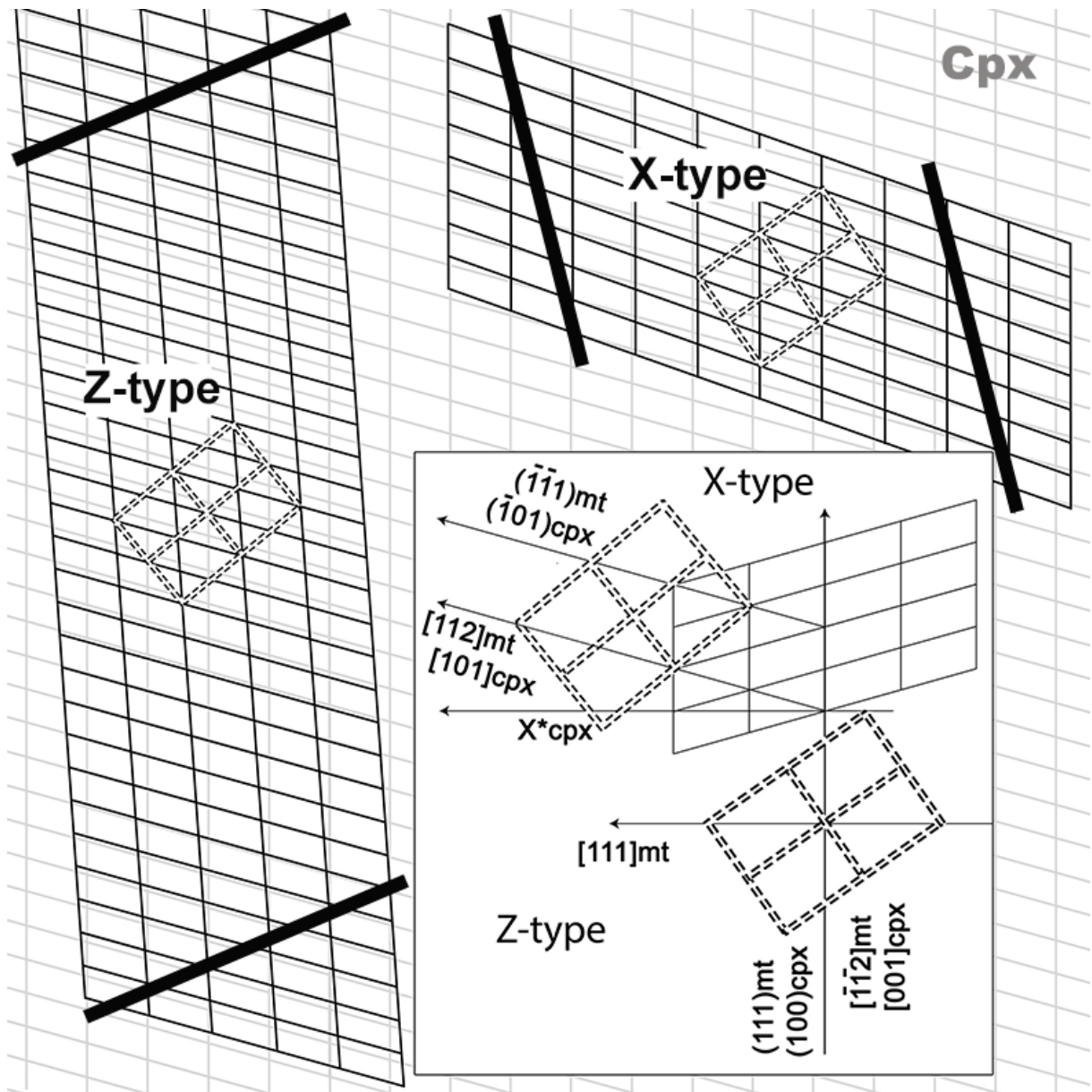
Figure 1. Schematic drawing of clinopyroxene lattice in terms of the alternative cell (grey solid lines), superimposed are magnetite lattices in terms of the alternative monoclinic cell in X-type and Z-type orientations (black solid lines), the heavy solid lines show interface orientations, where the $(100)_{cpx}$ planes are perfectly coherent with the $(111)_{mt}$ planes for the X-type inclusions and the $(-101)_{cpx}$ planes are perfectly coherent with the $(-1-11)_{mt}$ planes for the Z-type inclusions; the insert in the lower right shows the conventional magnetite cell (double dashed lines) viewed down the $[110]_{mt}$ –direction, which is parallel to the "b"-direction of clinopyroxene.

892